

Implementation of Flexible Embedded Nanowire Electrodes in Organic Light-Emitting Diodes

Lukas Kinner, Felix Hermerschmidt,* Theodoros Dimopoulos,* and Emil J. W. List-Kratochvil

The implementation of silver nanowires (NWs) as flexible transparent electrodes (FTEs) in solution-processed organic light-emitting diodes (OLEDs) still faces two major challenges: the high roughness of NW films and heat sensitivity of the most commonly used transparent substrate poly(ethylene terephthalate) (PET). A solution-based, roll-to-roll, and sheet-to-sheet scalable process to create indium tin oxide (ITO)-free FTEs is reported. This FTE is realized by spraying NWs on PET, without the necessity of postdeposition heat treatment. To overcome the roughness limitation, NW films are reverse transfer embedded on another PET substrate. As a result, the FTE shows a low roughness, as well as high mechanical, thermal, organic-solvent, and plasma stability. This developed FTE shows comparable transmittance with ITO but lower sheet resistance and higher mechanical stability. The FTE is implemented in a solution-processed OLED with PDY-132 (Super Yellow) as the emissive layer. In contrast to many other works in this field, a ZnO-nanoparticle electron-injection layer is used on the NWs instead of poly(3,4-ethylenedioxythiophene) polystyrene sulfonate (PEDOT:PSS) or other organic hole injectors. The use of ZnO nanoparticles instead of organic layers yields many advantages in terms of process and device stability. The resulting devices show greater flexibility, conductivity, and luminance than PET/ITO reference devices, while having the same power efficacy.

are easily achieved on glass substrates.^[1] Yet, the trend in industry is moving toward production on poly(ethylene terephthalate) (PET) substrates, because roll-to-roll (R2R) production offers faster production speeds than traditional bulk production of inorganic semiconductor devices, such as silicon solar cells.^[7,8] In consumer electronics, the trend goes toward flexible devices, like foldable smart phones or rollable screens.^[9]


However, ITO fails to deliver a low sheet resistance on PET due to the lower possible substrate temperature during the sputter deposition process and the high deposition rates necessary to achieve high conductivity.^[1] Typical PET/ITO foils show R_{sh} of $\approx 60 \Omega \text{ sq}^{-1}$. Further, ITO has the drawback of being brittle, which deteriorates its conductivity when subjected to mechanical strain.^[10] This fact compromises its use in flexible applications (e.g., bendable devices).^[11] Many different approaches for solution-processed TEs were brought forward in recent years to tackle the aforementioned drawbacks of ITO.

The use of inkjet-printed metal grids offers the possibility of producing already structured electrodes in an industrial-scale process.^[2,12–14] Other important TE materials include conductive polymers,^[15] ultrathin metallic layers,^[16] dielectric/metal/dielectric layers,^[8] carbon nanotubes,^[17] and metal nanowires (NWs).^[5,18]

The most widely used metal for NWs is silver. Silver NWs feature high transparency (90–96%), as well as low R_{sh} ($9\text{--}70 \Omega \text{ sq}^{-1}$).^[19] In addition to these optical and electrical

Modern optoelectronics, such as organic light-emitting diodes (OLEDs) and thin-film photovoltaics, rely on transparent electrodes (TEs).^[1–5] TEs assure that light can leave or reach the active materials (emitters or absorbers), while simultaneously serving to inject or extract the charge carriers. Indium tin oxide (ITO) is the industrial standard for TEs, due to its high optical transmittance in the visible spectral range ($>80\%$), together with its low sheet resistance (R_{sh}) of $<15 \Omega \text{ sq}^{-1}$.^[6] These key features

L. Kinner, Dr. F. Hermerschmidt, Prof. E. J. W. List-Kratochvil
Institut für Physik
Institut für Chemie & IRIS Adlershof
Humboldt-Universität zu Berlin
Brook-Taylor-Straße 6, 12489 Berlin, Germany
E-mail: felix.hermerschmidt@hu-berlin.de

 The ORCID identification number(s) for the author(s) of this article can be found under <https://doi.org/10.1002/pssr.202000305>.

© 2020 The Authors. Published by Wiley-VCH GmbH. This is an open access article under the terms of the Creative Commons Attribution-NonCommercial License, which permits use, distribution and reproduction in any medium, provided the original work is properly cited and is not used for commercial purposes.

DOI: 10.1002/pssr.202000305

L. Kinner, Dr. T. Dimopoulos
Center for Energy, Photovoltaic Systems
AIT Austrian Institute of Technology
Giefinggasse 6, 1210 Vienna, Austria
E-mail: theodoros.dimopoulos@ait.ac.at

Prof. E. J. W. List-Kratochvil
Helmholtz-Zentrum Berlin für Materialien und Energie GmbH
Brook-Taylor-Straße 6, 12489 Berlin, Germany

properties, NWs show excellent mechanical stability, which makes them a good candidate for flexible and R2R-processed electrodes.^[20] For R2R processing, different deposition methods for NWs have been presented, such as electrostatic spraying,^[21] wire bar coating,^[22] inkjet printing,^[23] air brush spraying,^[24] and spray coating.^[18]

Independent of the deposition technique, NW films feature two major drawbacks, namely their high roughness and their need for postdeposition treatments. High roughness is a bottleneck for thin-film device fabrication, as spikes from the one electrode may reach the opposing electrode and hence short circuit the device. Postdeposition treatments are necessary to remove the organic capping layer around NWs and assure silver–silver contact between the NWs. Both steps are necessary to reduce contact resistance between individual wires.^[25,26]

To overcome the roughness issue, different planarization and embedding processes have been put forward. Lian et al. proposed an embedding process for NWs, by pressing the spin-coated NWs into a poly(vinyl alcohol) (PVA) film, which was spin coated on a poly(ethylene naphthalate) substrate.^[25] Although the processing is straightforward and does not require vacuum processing, it is unclear if the PVA film resists solution processing, as the electrodes have been tested for evaporated OLEDs only.

A more stable approach for solution-processed embedded NWs was presented by Yu et al.^[27] NWs were drop cast on a host glass substrate, cured, and covered with a UV-curable poly (acrylate), which is peeled off of the sacrificial glass substrate, containing the NW film. The embedded NWs feature a low root-mean-square (RMS) roughness, as the new surface is the initial glass/NW interface. On the embedded electrode, a solution-processed OLED with the following architecture, poly(3,4-ethylenedioxythiophene):polystyrene sulfonate (PEDOT:PSS)/Super Yellow/CsF/Al, was tested. The presented devices feature a similar current efficacy performance to ITO, but lower electrical currents and lower luminance, compared with ITO.

Finally, Jung et al. presented an R2R process to create embedded and transferred NW electrodes.^[28] The NWs were wire-bar-coated on the host substrate (thermally stable polyimide [PI]) and thermally cured with an infrared dryer. It was shown that areas up to $45 \times 15 \text{ cm}^2$ had a homogeneous sheet resistance distribution. Then the NWs were embedded in a UV-curable polymer, while simultaneously transferring them to a new PET substrate (final substrate). It was shown that an evaporated OLED on this electrode achieved the same luminance but higher efficacy than a glass/ITO-based reference. Electrode performance in this case was largely influenced by the use of high-aspect-ratio NWs (length of 27 μm and width of 32 nm).

Recently, we have shown that sprayed and embedded NW electrodes in the UV-curable polymerOrmocomp (“Ormocomp” is a trademark of micro resist technology) can be obtained using PET as both host and target substrate.^[18] This approach avoids the use of an expensive PI host substrate and yields a conductive substrate that is compatible to solution processing of organic devices. Further, it is compatible with R2R and sheet-to-sheet processing. Sprayed NW electrodes have already been shown for sizes up to $10 \times 10 \text{ cm}^2$, only limited by the hot plate size used in the study.^[29] In the work presented here, we prove the applicability of this embedded electrode on PET in solution-processed OLED devices. The previously presented devices use either PEDOT:PSS or

evaporated hole-injection layers on the NWs to manufacture OLEDs. In the presented work a mixture of ZnO nanoparticles and polyethyleneimine (PEI) is used as electron-injection layer on NWs, creating an inverted OLED architecture.

A PEDOT:PSS-free OLED is less prone to humidity and has an additional encapsulating effect by ZnO. Furthermore, it is not necessary to apply many thin organic interlayers, which are difficult to control during processing and the inverted architecture offers better applicability in display production.^[30]

We prove the applicability of this embedded electrode on PET in solution-processed OLED devices. The presented inverted OLEDs on embedded NWs show the same power efficacy as ITO-based devices but a luminance which surpasses devices on standard PET/ITO substrates.

For comparison, we initially produced OLEDs with nonembedded sprayed NW films on PET. All devices were short circuited, due to a NW film roughness of 46 nm. Hence a planarization process, based on the embedding of the NWs into theOrmocomp layer, was used.^[18] The schematic of the process is shown in **Figure 1a**. NWs are sprayed on PET at 110 °C (step I). Elevated substrate temperature during spraying allows faster drying of the spray solution droplets. This in turn prevents coalescence to larger droplets and thereby increases homogeneous film morphology.^[31] For the case of PET, Scardaci et al. showed that a substrate temperature of 110 °C shows optimum conditions.^[29] At this temperature no deformation of the PET substrate was observed, as the continuous air and solution flow cools the PET substrate during spraying. Following the spraying, NWs are drop coated withOrmocomp (step II). On top of this arrangement the final substrate [PET, coated withOrmoprime 08 (“Ormoprime” is a trademark of micro resist technology)] is placed and then illuminated with UV light (step III). Then a lift-off is conducted, yielding NWs embedded inOrmocomp on PET (step IV).

To characterize the optical properties of the obtained electrode, optical transmittance measurements were carried out. In **Figure 1b** transmittance spectra of the NW films on PET at various process steps are shown. The dashed orange line shows the spectrum of the sprayed film after step I. Due to spraying of the NWs at 110 °C substrate temperature, the organic capping is removed during spraying and the resulting films have an R_{sh} of $13 \Omega \text{ sq}^{-1}$. Spraying NWs without substrate heating yielded films with $R_{\text{sh}} > 200 \text{ k}\Omega \text{ sq}^{-1}$. Spectra of NW films embedded inOrmocomp show an additional dip in the transmittance spectrum of the electrode at $\approx 400 \text{ nm}$ (light blue line), due to the light absorption from theOrmocomp layer. Overcoating the embedded NWs with the electron-injecting ZnO:PEI mixture does not change the transmittance significantly (dark blue line). It was observed that most NW device samples initially shorted or showed high dark currents, although the NWs were embedded. Hence, the embedded NW films were plasma treated to improve the wetting and reduce remaining NW spikes, before spin coating them with ZnO:PEI. Plasma treatment improved the number of working devices and individual device performance. PET/ITO samples were also plasma treated prior to ZnO:PEI coating to enhance the wetting and the work function. In the visible spectral wavelength range NW electrodes coated with ZnO:PEI show a slightly lower transmittance than PET/ITO electrodes coated with ZnO:PEI, but a far lower sheet resistance, as the ITO-based electrode has an R_{sh} of $60 \Omega \text{ sq}^{-1}$.

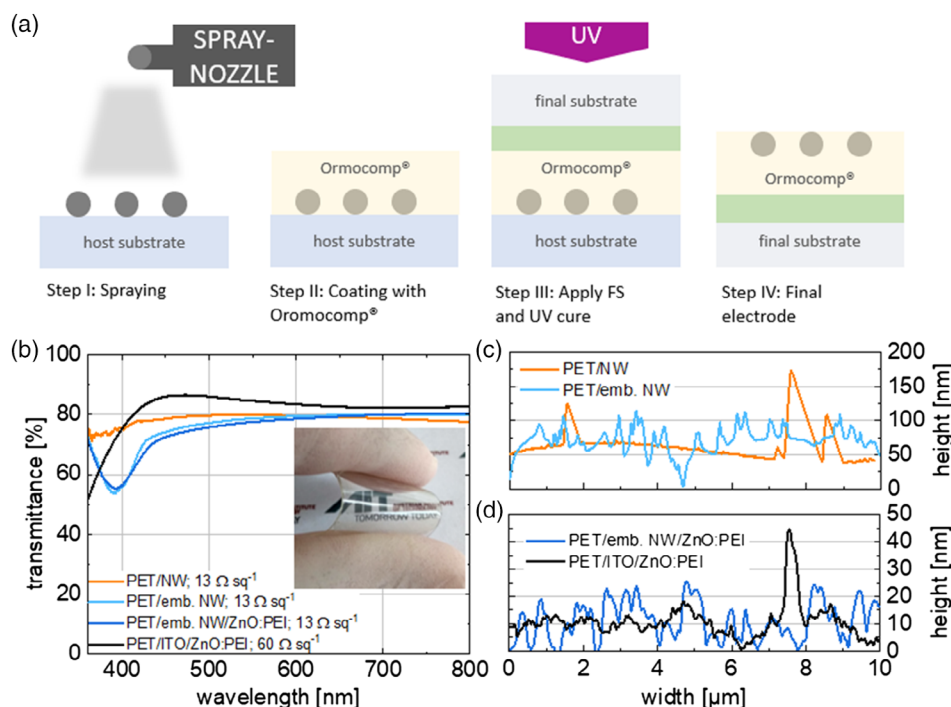


Figure 1. a) Schematic of the production process of the embedded NW electrodes: spraying (Step I), overcoating with Ormocomp (Step II), UV curing with Ormoprime 08 (green layer)-coated final substrate (Step III), final electrode (Step IV). b) Transmittance spectra of the different electrodes showing a transmittance of the developed electrode close to ITO; the inset shows the developed electrode. c) SFM line profile of nonembedded and embedded NWs, showing the reduction of large spikes. d) SFM profile of NW and ITO electrodes with ZnO:PEI, showing a further reduction of large spikes, which may occur on PET/ITO substrates.

As described earlier, devices with nonembedded NW electrodes showed short circuits due to RMS roughness of 46 nm. Scanning force microscopy (SFM) measurements were carried out to quantify the roughness decrease caused by embedding. The results are shown in Figure 1c. The height profile of the nonembedded NW film (orange line) shows significantly higher spikes, indicating higher roughness than the embedded NW films (light blue). The embedded electrodes show however some holes in the embedding polymer, caused by plasma treatment. Figure S1 in the Supporting Information shows an SFM image of the embedded NW electrode before plasma treatment, with no holes visible. Further details on the process and the effects of the plasma treatment can be found in a previous study.^[18] These holes are partially filled by the spin-coated ZnO:PEI layer (Figure 1d, dark blue). For comparison, also the profile of the ITO/ZnO:PEI electrode (black) is shown. To get a bigger picture of the roughness of the NW electrodes than just line profiles, confocal laser microscopy and SFM images are shown in **Figure 2**.

From confocal laser microscopy (Figure 2a) the RMS roughness of a $330 \times 330 \mu\text{m}^2$ area of the embedded NW electrode is shown to be ≈ 30 nm. A more detailed ($12 \times 12 \mu\text{m}^2$) SFM image of the same sample is shown in Figure 2b, indicating an RMS roughness of 25 nm. The high roughness value is mainly caused by holes in the Ormocomp from the plasma treatment and not by the sharp spikes which may cause shunts.^[18] By overcoating the embedded NW with ZnO:PEI (Figure 2c), an even smoother surface (RMS = 8.1 nm) is formed, which is close to the ITO/ZnO:PEI roughness of 5 nm (Figure S2, Supporting Information).

Having now confirmed that the developed electrode surface roughness is almost as low as the roughness of ITO and hence low enough for device manufacturing, the mechanical behavior was investigated.

One method to do so is by conducting bending tests on the electrode and investigating the measured resistance as a function of bending strain and bending cycles. The electrode resistance R was measured initially (R_0) and then after each iteration of bending cycles n . The tensile strain ϵ during bending is given by the formula: $\epsilon = d(2r)^{-1}$, where r is the bending radius and d the substrate thickness.^[32–35] For these experiments, $r = 4$ mm and the substrate thickness d (Ormocomp + PET) equals $480 \mu\text{m}$, which yields 6% tensile film strain. In addition, to tensile bending, compressive bending (film inside the curvature) was conducted. Figure 2d shows the mechanical stability of the embedded electrode in comparison with ITO. R_{sh} of ITO increases 30 times within 70 compressive bending cycles, whereas the NW electrode showed no change in R_{sh} for compressive bending at $R_{\text{bend}} = 4$ mm for 5000 cycles. At the same bending radius in tensile bending, R_{sh} increased only three times over 5000 circles, which is ten times less than ITO. R_{sh} changes strongly in tensile bending compared with compressive bending because tensile bending is more strenuous for the film.^[32,33] The SEM images of the ITO and NW electrodes before and after bending (Figure S3) show the strong contrast in morphology, explaining the observed difference in R_{sh} . While ITO films contain visible cracks after bending, the NW electrode shows no such damage.

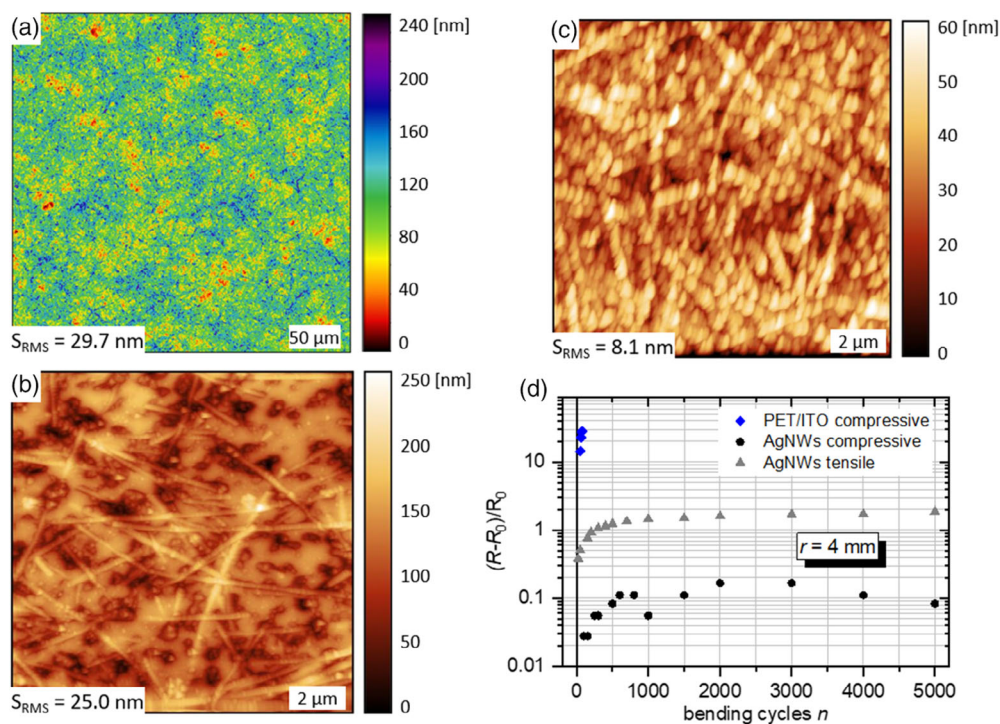


Figure 2. a) Large-area surface morphology of the electrode, b) SFM image of embedded NW electrode showing holes in the electrode due to plasma treatment, c) SFM image of embedded NW electrode, coated with ZnO:PEI, showing lower roughness, and d) bending tests of the NW electrode and commercial ITO substrates showing the much higher mechanical stability of the NW electrode.

Utilizing both ITO and NW-based electrodes, OLEDs were fabricated, and their performance was investigated. To do so, current density J and luminance L were measured as a function of applied voltage V to determine the so-called J - V - L curves. **Figure 3** shows the performance data of OLEDs manufactured on embedded NW FTEs, as well as on PET/ITO reference substrates. In **Figure 3a** the corresponding J - V characteristics of the devices are shown. The NW-based devices show up to two orders of magnitude higher dark currents, caused by remaining shunts through the light-emitting layer. In the range from 2 to 4 V, devices based on NW electrodes show similar electrical behavior to the ITO reference devices. Starting at 4 V, the NW-based devices show a higher current increase as the ITO reference devices. The sheet resistance of the NW electrode is ≈ 5 times lower than the ITO electrode. This results in a faster current increase. Similar behavior of current increase in OLEDs on NWs, compared with ITO devices, has been shown in literature for a comparable device architecture.^[36] It is important to point out that the saturation current of the NW devices is higher than that of ITO devices. This behavior also results from the five times lower R_{sh} of the NW electrode, compared with the ITO reference electrode.

In **Figure 3b** the luminance characteristics corresponding to the J - V characteristics in **Figure 3a** are shown. At 4.5 V, the luminance values of the NW devices exceed the ITO reference devices. One can conclude that the higher luminance starting at 4.5 V is caused by the higher currents starting at 4 V (**Figure 3a**). As stated earlier, this is derived from the lower R_{sh} of the NW electrode. The maximum luminance of embedded NW electrode devices was $34\,000\text{ cd m}^{-2}$, whereas the ITO reference device reached

a maximum luminance of 5000 cd m^{-2} ; both values were achieved at 7 V. At 7 V the current density of the NW device is a factor 7 higher than the current density of the ITO device, correlating with the five times lower sheet resistance of the NW electrode. This results in the seven times higher luminance value.

Power efficacy (lm W^{-1}) of the devices was determined by calculating the electrical power consumed by the OLED ($P = IU$) and calculating lm from cd according to Forrest et al. by assuming a Lambertian light source: $1\text{ lm} = \pi (1\text{ cd})$.^[37]

The resulting power efficacy over luminance graph is shown in **Figure 3c**. At lower luminance the ITO reference device shows a higher efficacy. This results from the fact that at lower current densities ITO-based devices show higher luminance values than the NW-based devices. The highest power efficacy is achieved by the ITO reference device with 2.2 lm W^{-1} at 5000 cd m^{-2} , whereas the highest efficacy of embedded NW devices is also 2.2 lm W^{-1} but at a considerably higher luminance value of $34\,000\text{ cd m}^{-2}$. This same efficacy of the NW electrode device results from the higher luminance at higher current densities, which is achieved due to its lower R_{sh} . This indicates that our OLED architecture is in general able to achieve these efficacies and efficiently convert higher currents to higher luminance values, as previously shown. Similar behavior has been shown in OLEDs with a comparable architecture in the literature.^[36]

One can conclude that the ITO-based devices have a higher power efficacy at lower current densities and resulting lower luminance due to lower leakage. However, this advantage over the NW-based electrode is lost at higher current densities and the resulting higher luminance, when R_{sh} plays a larger role

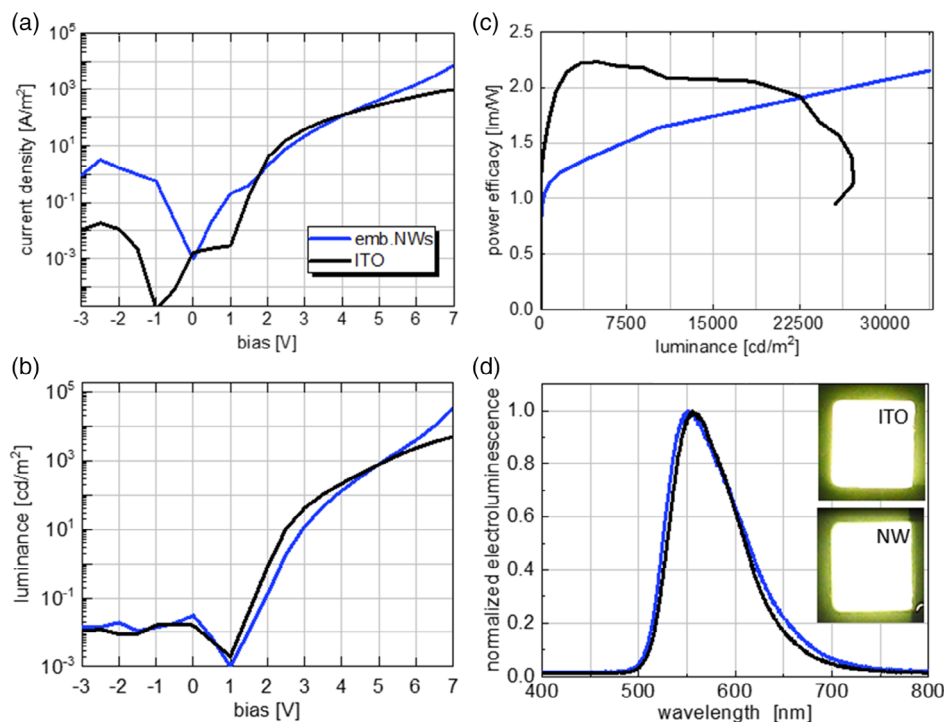


Figure 3. Characteristics of OLED devices using the embedded NW electrodes on PET and a PET/ITO reference. a) Current density versus bias voltage, b) luminance versus bias voltage, c) power efficacy versus luminance, and d) electroluminescence spectra of OLEDs; the insets show the working devices on ITO and NW electrodes, respectively.

and ohmic losses in the ITO-based devices become more important than the initial leakage losses in the NW-based devices.

Finally, to analyze the color of the light source depending on the electrode type, electroluminescence (EL) spectra were taken of both device types. Independently of the electrode, both device types show the same EL spectra (Figure 3d), with the Commission Internationale de l'Éclairage (CIE) coordinates: $x = 0.44$ and $y = 0.54$ for the NW electrode and $x = 0.45$ and $y = 0.54$ for the ITO reference. This indicates the same light out-coupling properties of both electrode types, as well as the same chemical stability for both types because no color changing degradation of the light-emitting layer is observed.

In conclusion we have demonstrated a NW-based ITO-free FTE, implemented in a solution-processed OLED. Our work shows a vacuum-free way to process NW films on PET to obtain FTEs with a sheet resistance five times lower than that of ITO, while offering similar transmittance. In terms of flexibility the developed electrode shows no resistance change in compressive bending and only three times increase over 5000 tensile bending cycles with 6% strain, whereas the comparison ITO electrode shows large resistance increases after 70 bending cycles.

During device studies it was shown that the presented electrode works well with a solution-processed ZnO:PEI electron-injection layer to realize an efficient inverted OLED architecture. It was further shown that plasma treatment can reduce possible shunts in NW-based electrodes. In device tests our electrode showed similar power efficacy performance as commercial ITO PET substrates, but almost a seven times higher maximum luminance values. Overall, a flexible and solution-processed alternative to ITO was presented.

Experimental Section

Fabrication of NW Electrodes: The fabrication of the embedded NW electrodes was realized following the process described in a previous study.^[18] Clogging of the spraying nozzle by the NWs was not observed, because the nozzle diameter (≈ 3 mm) was far larger than the average NW length (10 μ m), and in contrast to inkjet printing, spraying is a continuous process, which prevents the drying of the solution at any place in the tubing system. Further, the shaping air was set to its highest value, which removed almost all NW residuals from the nozzle surface. The film was kept uniform by choosing the spraying pattern over the substrate in a zig-zag form and having a small offset at the start of every new spraying circle. The amount of wires on the substrate and therefore the “thickness” was set by the number of spraying circles. Further details are found in a previous study.^[18] To match the contacts of the OLED measurement setup, the devices were patterned during spraying by covering the sides with Kapton tape to leave a 5 mm-wide middle strip of the conducting NW film; then, Cr/Au fingers were evaporated.

OLED Manufacturing: To reduce the remaining spikes of NWs and optimize wetting behavior, all samples were plasma treated in a Femto Diener Plasma tool. Ambient air was used as plasma gas at a pressure of 0.3 mbar and 100 W power for 4 min. Following the plasma treatment, the samples were spin coated with a ZnO:PEI (2:1 by volume) in isopropyl alcohol (IPA) solution with 2500 rpm for 60 s and heated for 10 min at 110 °C. The ZnO nanoparticle solution was purchased from Genesink, whereas PEI was purchased from Sigma Aldrich, and the PEI solution prepared according to the recipe of Zhou et al.^[38] The emitting layer PDY-132 (Super Yellow, Merck) was spun at 2500 rpm for 60 s from a 5 mg mL⁻¹ toluene solution, with no heating applied. Following the spin-coating steps, 10 nm MoO₃ and 200 nm Ag were evaporated. All processing and measuring except the vacuum steps were conducted in ambient air.

Characterization Methods: The sample surfaces were characterized with a scanning force microscope (Molecular Imaging, Pico Plus) in tapping mode, using tapping mode cantilevers (PPP-NCHR) from

Nanosensors. The images were analyzed using open-source software (Gwyddion). Laser confocal microscopy images were taken with an Olympus LEXT OLS4100. For optical transmittance measurements a Bruker Vertex 70 Fourier-transform (FT) spectrometer, equipped with an additional visible light source was used. For the wavelength range 330–550 nm a GaP detector was used and for the range 550–1150 nm a Si detector. Transmittance was measured with a teflon-coated integration sphere from Bruker. During bending tests, the resistance was measured from one edge of the sample to the other, perpendicular to the strain direction.

Current density/voltage/luminance device characterization was conducted with a Keithley 2450 source measurement unit, together with a Konica Minolta LS-160 luminance meter in a purpose-built setup. The EL spectra were measured with an Ocean Optics CS2000 spectrometer and recorded using Ocean View software.

Supporting Information

Supporting Information is available from the Wiley Online Library or from the author.

Acknowledgements

This work was partially funded by the Austrian Climate Fund project flex!PV_2.0 (project number 853603). This work was conducted in the framework of the Joint Lab GEN_FAB and was supported by the HySPRINT innovation lab at Helmholtz-Zentrum Berlin. Open access funding enabled and organized by Projekt DEAL.

Conflict of Interest

The authors declare no conflict of interest.

Keywords

flexible materials, indium tin oxide free, organic light-emitting diodes, poly(ethylene terephthalate), transparent electrodes

Received: June 17, 2020

Revised: July 16, 2020

Published online: August 11, 2020

- [1] A. I. Hofmann, E. Cloutet, G. Hadziioannou, *Adv. Electron. Mater.* **2018**, *4*, 1700412.
- [2] F. Hermerschmidt, I. Burgués-Ceballos, A. Savva, E. D. Sepos, A. Lange, C. Boeffel, S. Nau, E. J. W. List-Kratochvil, S. A. Choulis, *Flex. Print. Electron.* **2016**, *1*, 035004.
- [3] F. Hermerschmidt, S. A. Choulis, E. J. W. List-Kratochvil, *Adv. Mater. Technol.* **2019**, *4*, 1800474.
- [4] S. De, T. M. Higgins, P. E. Lyons, E. M. Doherty, P. N. Nirmalraj, W. J. Blau, J. J. Boland, J. N. Coleman, *ACS Nano* **2009**, *3*, 1767.
- [5] S. Naghdi, K. Rhee, D. Hui, S. Park, *Coatings* **2018**, *8*, 278.
- [6] Y. R. Jang, W. H. Chung, Y. T. Hwang, H. J. Hwang, S. H. Kim, H. S. Kim, *ACS Appl. Mater. Interfaces* **2018**, *10*, 24099.
- [7] C. G. Granqvist, *Sol. Energy Mater. Sol. Cells* **2012**, *99*, 1.
- [8] L. Kinner, M. Bauch, R. A. Wibowo, G. Ligorio, E. J. W. List-Kratochvil, T. Dimopoulos, *Mater. Des.* **2019**, *168*, 107663.
- [9] M. Luo, Y. Liu, W. Huang, W. Qiao, Y. Zhou, Y. Ye, L.-S. Chen, *Micromachines* **2017**, *8*, 12.
- [10] J. Li, Y. Tao, S. Chen, H. Li, P. Chen, M.-z. Wei, H. Wang, K. Li, M. Mazzeo, Y. Duan, *Sci. Rep.* **2017**, *7*, 16468.
- [11] R. P. Xu, Y. Q. Li, J. X. Tang, *J. Mater. Chem. C* **2016**, *4*, 9116.
- [12] E. Georgiou, S. A. Choulis, F. Hermerschmidt, S. M. Pozov, I. Burgués-Ceballos, C. Christodoulou, G. Schider, S. Kreissl, R. Ward, E. J. W. List-Kratochvil, C. Boeffel, *Sol. RRL* **2018**, 1700192.
- [13] S. M. Pozov, G. Schider, S. Voigt, F. Ebert, K. Popovic, F. Hermerschmidt, E. Georgiou, I. Burgués-Ceballos, L. Kinner, D. Nees, B. Stadlober, C. Rapley, R. Ward, S. A. Choulis, E. J. W. List-Kratochvil, C. Boeffel, *Flex. Print. Electron.* **2019**, *4*, 025004.
- [14] L. Kinner, S. Nau, K. Popovic, S. Sax, I. Burgués-Ceballos, F. Hermerschmidt, A. Lange, C. Boeffel, S. A. Choulis, E. J. W. List-Kratochvil, *Appl. Phys. Lett.* **2017**, *110*, 101107.
- [15] Y. H. Kim, J. Lee, S. Hofmann, M. C. Gather, L. Müller-Meskamp, K. Leo, *Adv. Funct. Mater.* **2013**, *23*, 3763.
- [16] K. Ellmer, *Nat. Photonics* **2012**, *6*, 808.
- [17] D. S. Hecht, L. Hu, G. Irvin, *Adv. Mater.* **2011**, *23*, 1482.
- [18] L. Kinner, E. J. W. List-Kratochvil, T. Dimopoulos, *Nanotechnology* **2020**, *31*, 365303.
- [19] P. Lee, J. Lee, H. Lee, J. Yeo, S. Hong, K. H. Nam, D. Lee, S. S. Lee, S. H. Ko, *Adv. Mater.* **2012**, *24*, 3326.
- [20] Y. Jin, D. Deng, Y. Cheng, L. Kong, F. Xiao, *Nanoscale* **2014**, *6*, 4812.
- [21] T. Kim, A. Canlier, G. H. Kim, J. Choi, M. Park, S. M. Han, *ACS Appl. Mater. Interfaces* **2013**, *5*, 788.
- [22] N. de Guzman, J. Lopez, M. Vasquez Jr., M. D. Balela, *Mater. Sci. Forum* **2017**, *890*, 89.
- [23] P. Maisch, K. C. Tam, L. Lucera, H. J. Egelhaaf, H. Scheiber, E. Maier, C. J. Brabec, *Org. Electron. Phys. Mater. Appl.* **2016**, *38*, 139.
- [24] T. Akter, W. S. Kim, *ACS Appl. Mater. Interfaces* **2012**, *4*, 1855.
- [25] L. Lian, D. Dong, D. Feng, G. He, *Org. Electron.* **2017**, *49*, 9.
- [26] S. Bai, H. Wang, H. Yang, H. Zhang, X. Guo, *Mater. Res. Express* **2018**, *5*, 026406.
- [27] Z. Yu, Q. Zhang, L. Li, Q. Chen, X. Niu, J. Liu, Q. Pei, *Adv. Mater.* **2011**, *23*, 664.
- [28] E. Jung, C. Kim, M. Kim, H. Chae, J. H. Cho, S. M. Cho, *Org. Electron. Phys. Mater. Appl.* **2017**, *41*, 190.
- [29] V. Scardaci, R. Coull, P. E. Lyons, D. Rickard, J. N. Coleman, *Small* **2011**, *7*, 2621.
- [30] R. Kacar, S. P. Mucur, F. Yildiz, S. Dabak, E. Tekin, *Nanotechnology* **2017**, *28*, 245204.
- [31] M. Majumder, C. Rendall, M. Li, N. Behabtu, J. A. Eukel, R. H. Hauge, H. K. Schmidt, M. Pasquali, *Chem. Eng. Sci.* **2010**, *65*, 2000.
- [32] S. Aura, V. Jokinen, M. Laitinen, T. Sajavaara, S. Franssila, *J. Micromech. Microeng.* **2011**, *21*, 125003.
- [33] O. Glushko, A. Klug, E. J. W. List-Kratochvil, M. J. Cordill, *J. Mater. Res.* **2017**, *32*, 1760.
- [34] O. Glushko, A. Klug, E. J. W. List-Kratochvil, M. J. Cordill, *Mater. Sci. Eng. A* **2016**, *662*, 157.
- [35] O. Glushko, M. J. Cordill, A. Klug, E. J. W. List-Kratochvil, *Microelectron. Reliab.* **2016**, *56*, 109.
- [36] S. J. Lee, Y. H. Kim, J. K. Kim, H. Baik, J. H. Park, J. Lee, J. Nam, J. H. Park, T. W. Lee, G. R. Yi, J. H. Cho, *Nanoscale* **2014**, *6*, 11828.
- [37] S. R. Forrest, D. D. C. Bradley, M. E. Thompson, *Adv. Mater.* **2003**, *15*, 1043.
- [38] Y. Zhou, C. Fuentes-Hernandez, J. Shim, J. Meyer, A. J. Giordano, H. Li, P. Winget, T. Papadopoulos, H. Cheun, J. Kim, M. Fenoll, A. Dindar, W. Haske, E. Najafabadi, T. M. Khan, H. Sojoudi, S. Barlow, S. Graham, J. Brédas, S. R. Marder, A. Kahn, B. Kippelen, *Science* **2012**, *873*, 327.